Photochemistry of Adsorbed Nitrate Formed From Nitric Acid Adsorption on α-Fe2O3 Particle Surfaces: The Role of Adsorbed Water in the Formation of Nitrogen-Reduced Surface Species.

ARTICLE *in* THE JOURNAL OF PHYSICAL CHEMISTRY A · DECEMBER 2013

Impact Factor: 2.69 · DOI: 10.1021/jp409017m · Source: PubMed

5 AUTHORS, INCLUDING:

Pradeep M Jayaweera

34 PUBLICATIONS **495** CITATIONS

SEE PROFILE

Gayan Rubasinghege

New Mexico Institute of Mining and Technology

15 PUBLICATIONS **284** CITATIONS

SEE PROFILE

THE JOURNAL OF PHYSICAL CHEMISTRY A

Article

pubs.acs.org/JPCA

Surface Photochemistry of Adsorbed Nitrate: The Role of Adsorbed Water in the Formation of Reduced Nitrogen Species on α-Fe_2O_3 Particle Surfaces

Charith E. Nanayakkara,[†,∥] Pradeep M. Jayaweera,[‡,∥] Gayan Rubasinghege,[†] Jonas Baltrusaitis,[§] and Vicki H. Grassian*[,†]

[†]Department of Chemistry, University of Iowa, Iowa City, Iowa 52242, United States

[‡]Department of Chemistry, University of Sri Jayewardenepura, Nugegoda, Sri Lanka

[§]Photocatalytic Synthesis Group, Faculty of Science and Engineering, University of Twente, 7500 AE, Enschede, The Netherlands

Supporting Information

ABSTRACT: The surface photochemistry of nitrate, formed from nitric acid adsorption, on hematite (α-Fe_2O_3) particle surfaces under different environmental conditions is investigated using X-ray photoelectron spectroscopy (XPS). Following exposure of α-Fe_2O_3 particle surfaces to gas-phase nitric acid, a peak in the N1s region is seen at 407.4 eV; this binding energy is indicative of adsorbed nitrate. Upon broadband irradiation with light (λ > 300 nm), the nitrate peak decreases in intensity as a result of a decrease in adsorbed nitrate on the surface. Concomitant with this decrease in the nitrate coverage, there is the appearance of two lower binding energy peaks in the N1s region at 401.7 and 400.3 eV, due to reduced nitrogen species. The formation as well as the stability of these reduced nitrogen species, identified as NO^- and N^-, are further investigated as a function of water vapor pressure. Additionally, irradiation of adsorbed nitrate on α-Fe_2O_3 generates three nitrogen gas-phase products including NO_2, NO, and N_2O. As shown here, different environmental conditions of water vapor pressure and the presence of molecular oxygen greatly influence the relative photoproduct distribution from nitrate surface photochemistry. The atmospheric implications of these results are discussed.

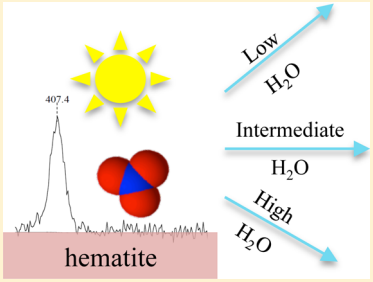

INTRODUCTION

Nitrate ion is an important chromophore and can undergo photochemical reactions on the surface of atmospheric aerosols,[1] deliquesced thin films,[2] ice/snow,[3−6] and in solution.[7−9] Nitrate ion has an absorption maximum at 302 nm (ε = 7.2 mol dm^{-3} cm^{-1}) in aqueous solution.[10] In the atmosphere, gas-phase nitrogen oxides readily react with particulate matter (e.g., mineral dust) to yield adsorbed nitrate. Atmospheric nitric acid is the main reservoir species in the NOx cycle. Heterogeneous reactions and possible renoxification mechanisms of tropospheric HNO_3 acid have been widely studied on different environmental interfaces and surfaces.[11−16] Mineral dust aerosols act as a reactive surface for atmospheric nitric acid adsorption and photochemical reactions of adsorbed nitrate.

The photochemistry of adsorbed nitrate, formed by either exposure to NO_2 or HNO_3, has been widely studied on the surface of components of mineral dust aerosol.[17−20] Photoexcitation of adsorbed nitrates forms several gas-phase products like N_2O, NO, and NO_2 and HONO.[18,20,21] For example, transmission FTIR studies of HNO_3 reacted γ-Al_2O_3 particles observed gas-phase NO and NO_2 formation as the main gas-phase products upon irradiation with λ > 300 nm light.[18] Irradiation of HNO_3 reacted in NaY zeolite showed formation of nitrite thought to be stabilized in the zeolite cage due to interactions with the charge compensating cation.[17] Additionally, some recent studies on NO_2 adsorption and photochemistry on semiconductor metal oxides such as Cr_2O_3 and TiO_2 have shown conversion of adsorbed nitrate to gas-phase NOx species under irradiation conditions.[19,20,22] These studies used chemiluminescence, mass spectrometry and infrared spectroscopy as tools to detect gas-phase photoproducts and infrared spectroscopy and X-ray photoelectron spectroscopy to detect adsorbed photoproducts as well. For adsorbed species, it is sometimes difficult to differentiate products due to the fact that there are overlapping absorption bands for different species that contain N−O functional groups.[23,24] X-ray photoelectron spectroscopy (XPS), however, can detect adsorbates that differ in the oxidation state of nitrogen atom. In this study XPS is used to investigate the surface photochemistry of nitrate adsorbed on hematite particle surfaces.

Hematite is one of the most common iron oxide polymorphs present in the Earth's crust. Iron-containing particles are transferred to the atmosphere from both wind and volcanic activities in the form of iron-containing mineral dust and volcanic ash aerosols.[25] Hematite is a semiconductor material with a lower band gap of 2.2 eV that can absorb solar radiation and has the potential to alter nitrate photochemistry path-

Received: September 9, 2013
Revised: November 27, 2013
Published: December 3, 2013

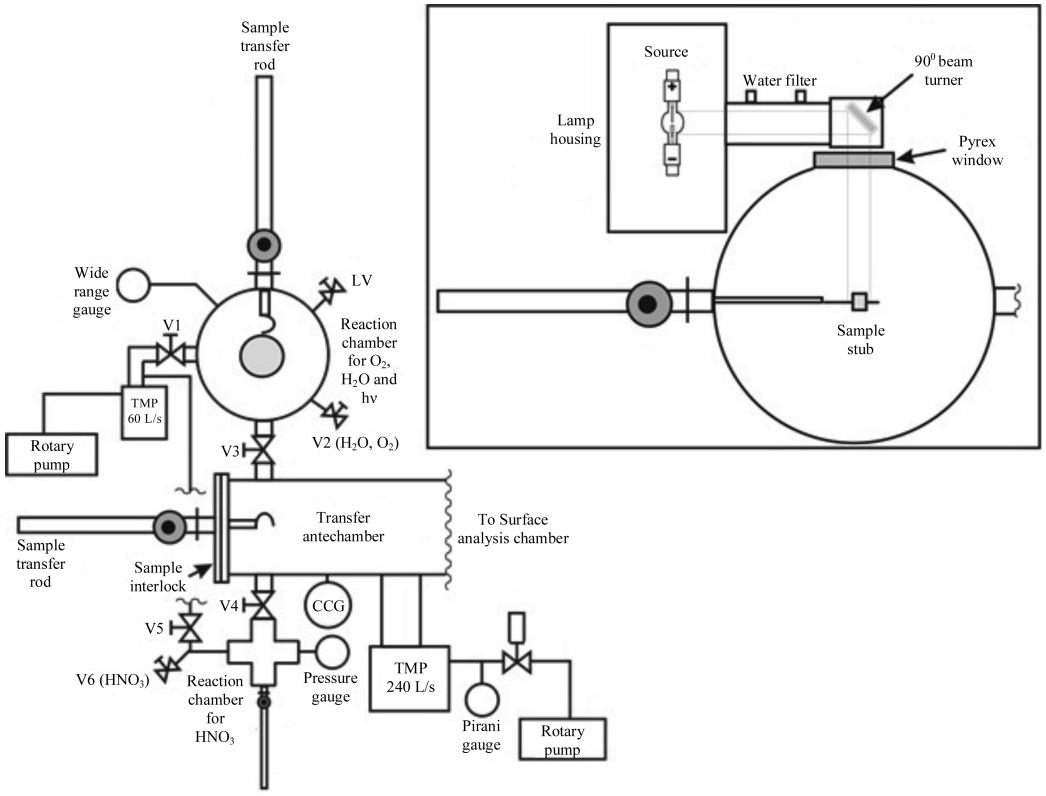

Figure 1. Schematic of the custom-designed Kratos Axis Ultra XPS system coupled with UV irradiation. The system consists of four chambers: a transfer antechamber, surface analysis chamber (not shown), reaction chamber and Teflon-coated HNO_3 reaction chamber. A cross section of the O_2/H_2O reaction chamber equipped with the UV source and beam optics is shown in the inset. See Experimental Methods for a more detailed description of this four chamber system. Note: TMP, turbomolecular pump; CCG, cold cathode gauge; LV, leak valve; and V, valve.

ways.[26] Therefore, understanding the surface photochemistry of nitrate adsorbed on hematite is important to further understand atmospheric processes. In this study, photochemistry of adsorbed nitrate on hematite, α-Fe_2O_3 surface is investigated under environmentally relevant relative humidity and molecular oxygen by XPS and FTIR spectroscopic techniques. Due to the importance of iron solubility in iron cycling,[27] the impact that this reaction has on iron dissolution is also investigated.

EXPERIMENTAL METHODS

Surface XPS Analysis Chamber Coupled with Transfer and Reaction Auxiliary Chambers. The custom-designed Kratos Axis Ultra X-ray photoelectron spectroscopy system for reactions and analysis has been described in detail before.[28] For these experiments, it was modified to accommodate an additional Teflon-coated reaction chamber for HNO_3 reaction experiments and UV source for photochemistry experiments.[28−30] The experimental setup has capabilities for reacting samples with gas-phase reactants and evacuating the gas-phase and surface product analysis with four different chambers that include: (i) an ultra high vacuum (UHV) surface analysis chamber, (ii) a sample transfer antechamber, (iii) a stainless steel reaction chamber, and (iv) a Teflon-coated reaction chamber (Figure 1). The transfer antechamber is connected to the analysis chamber, steel reaction chamber, and Teflon-coated reaction chamber. With this configuration, the transfer antechamber is used to introduce samples into the analysis chamber, and also allows for samples to be transferred directly from the surface analysis chamber to the reaction chambers and vice versa.

The Teflon-coated reaction chamber is connected to the transfer antechamber. The details of the stainless steel reaction chamber have been described before.[28] Additionally, a 500 W Hg lamp (Oriel Instruments model number 66033) was used to irradiate the samples in the steel reaction chamber. A water filter (Oriel Instruments) was used in line with the lamp output to minimize infrared damage and heating of the sample. The light from the lamp was reflected using a 90° turning mirror (Oriel Instruments, model: 66215 Beam Turning Mirror, Full Reflector, 200 nm−30 μm Primary Range, 1.5 Inch Series) into the reaction chamber via the Pyrex window. The transmissivity of the Pyrex window was ∼80% at the wavelengths above ∼320 nm with a 0.72 W/cm^2 measured light intensity at the sample.

For typical XPS analysis, powdered samples were pressed into indium foil and mounted onto a copper stub. After the initial scans at the surface analysis chamber were acquired, the sample was transferred to the Teflon-coated chamber via the transfer antechamber by means of sample transfer rod and a hand valve. The sample was then reacted with HNO_3. HNO_3 reacted α-Fe_2O_3 surfaces were evacuated and transferred to the sample analysis chamber for initial scans. The evacuation removes molecularly adsorbed HNO_3. After the initial scans, samples were transferred to the steel reaction chamber for reactions under environmentally relevant conditions of (1) H_2O, (2) O_2, and (3) H_2O/O_2 and UV light. No gas-phase HNO_3 was present in the chamber during those reactions. Reactant gas was introduced in approximately 15 s. The resulting gas mixture was allowed to equilibrate with the sample for at least 30 min. The reacted sample was then evacuated and

dx.doi.org/10.1021/jp409017m | J. Phys. Chem. A 2014, 118, 158−166

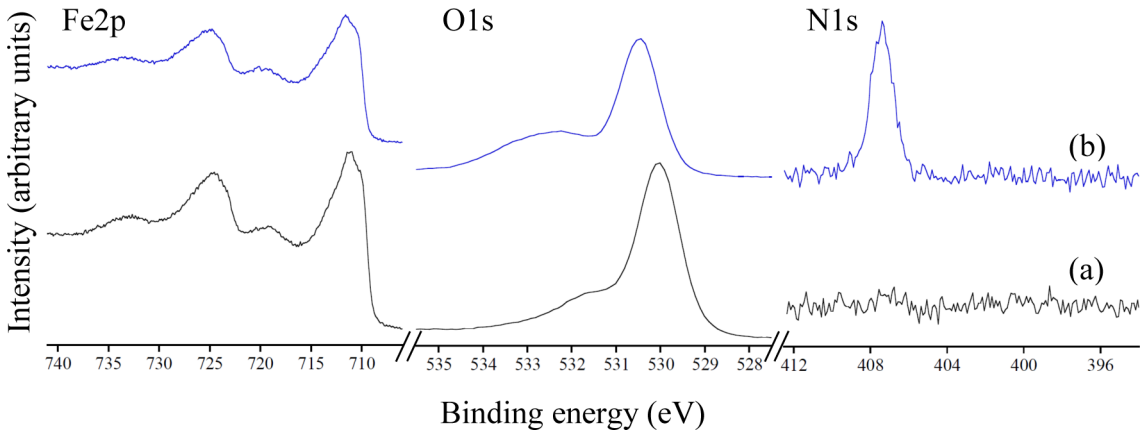

Figure 2. High-resolution X-ray photoelectron spectra of α-Fe_2O_3 particles in the Fe2p, O1s, and N1s binding energy regions (a) prior to and (b) after exposure to gas-phase HNO_3.

transferred back to the analysis chamber for postreaction surface characterization.

Data Processing of Core Photoelectron Spectra. All spectra were calibrated using the adventitious C1s peak at 285.0 eV. A Shirley-type background was subtracted from each spectrum to account for inelastically scattered electrons that contribute to the broad background. CasaXPS software was used to process the XPS data.[31] The N1s transition was fit to one peak with a fixed full-width-at-the-half-maximum (fwhm) value of 1.4 eV. The components of the peaks contain a Gaussian/Lorentzian product with 30% Lorentzian and 70% Gaussian character. An error of ±0.2 eV is reported for all peak binding energies.

Transmission FTIR Spectroscopy. For FTIR measurements, the α-Fe_2O_3 particles were prepared by pressing onto half of a tungsten grid (Buckbee Mears, 100 lines per inch tungsten mesh wire widths of ~0.0015 in. and thickness of ~0.002 in.). The other half of the grid was left blank for gas-phase measurements. The grid half coated with the oxide powder was placed inside the infrared cell. The inside of the stainless steel cube is coated with Teflon to avoid HNO_3 decomposition on the walls of the infrared cell. The oxide samples prepared on the tungsten grid are secured inside the infrared cell by Teflon-coated sample holder jaws. The infrared cell is connected to a vacuum chamber through a Teflon tube and two consecutive glass gas manifolds with ports for gas introduction and two absolute pressure transducers. Details of the experimental system have been described before.[32] Typically, 250 scans were collected with an instrument resolution of 4 cm^{-1} in the spectral range from 750 to 4000 cm^{-1}. Absorbance spectra for gas and adsorbed species were obtained by referencing single beam spectra of the blank grid and the oxide-coated grid to single beam spectra collected prior to gas exposure.

Iron Dissolution Experiments. HNO_3 reacted α-Fe_2O_3 particles were prepared in a Teflon-coated reaction chamber by reacting with HNO_3 to investigate the effect of HNO_3 on Fe dissolution. Reacted particles were suspended in optima water (Sigma Aldrich) at a mass loading of 30 mg/50 mL. The suspension was stirred for 24 h. The stability of unreacted and reacted particle suspensions was measured using the sedimentation plots by measuring the extinction with a Perkin-Elmer Lambda 20 UV−visible spectrometer at 510 nm. Iron dissolution was studied for both unreacted and HNO_3 reacted α-Fe_2O_3. An aliquot from the supernatant suspension was passed through a 0.2 μm PTFE filter to remove particles. The concentration of iron was measured using a Varian 720-ES inductively coupled plasma-optical emission spectrometer (ICP-OES). Dissolution of unreacted α-Fe_2O_3 was also conducted under the same conditions for comparison. All experiments were conducted in triplicate.

Characterization of α-Fe_2O_3. X-ray diffraction (XRD), scanning electron microscopy (SEM), and BET surface area analyzer were used to characterize the α-Fe_2O_3 samples.

Sources of Chemicals. Dry gaseous nitric acid was taken from the vapor of a 1:3 mixture of concentrated HNO_3 (70.6% HNO_3, Mallinckrodt) and 95.9% H_2SO_4 (Mallinckrodt). For relative humidity studies, distilled H_2O (Milli-Q) was used. Prior to use, both the distilled water and the HNO_3 were degassed several times with consecutive freeze−pump−thaw cycles. Oxygen (UPC grade) was obtained from Airgas. Hematite (α-Fe_2O_3, Alfa Aesar, α-phase, 99% metal basis) was used as received.

RESULTS AND DISCUSSION

Characterization of α-Fe_2O_3. The X-ray diffraction pattern of α-Fe_2O_3 shown in Supporting Information Figure S1(a) agrees well with the standard pattern for hematite. The average particle size of α-Fe_2O_3 was determined by scanning electron microscopy (SEM) and shows particles with diameter of 310 ± 22 nm (200 particles counted). Supporting Information Figure S1(b) shows an SEM image of the α-Fe_2O_3 particles used. Surface area measurements using BET analysis showed a specific surface area of 23 ± 2 m^2/g.

XPS of Metal−Nitrogen Salt Standards. To establish characteristic binding energies that may help to identify surface species generated from HNO_3 adsorption on α-Fe_2O_3 surfaces, the results of previously measured N1s binding energies for nitrogen containing salts were used here. In particular, a single peak at 407.4 eV was observed for $NaNO_3$ and was assigned to the N1s transition in nitrate ion (NO_3^-), and similarly a single peak was observed in the N1s region for $NaNO_2$ at 403.6 eV, assigned to N1s transition in adsorbed nitrite (NO_2^-).[28] Torres et al. have reported that the N1s peak of iron nitride (FeN) appeared at 397.4 eV.[33] These three reference compounds encompass a full range of N1s binding energies for HNO_3 reaction product related compounds, as the nitrogen oxidation state changes from +5 on $NaNO_3$ to −3 in FeN, thus accounting for all possible nitrogen oxidation states. The binding energy decreases with the decrease in the nitrogen

dx.doi.org/10.1021/jp409017m | J. Phys. Chem. A 2014, 118, 158−166

oxidation state due to the increase in number of electrons as well as the electron−electron repulsion.

XPS of HNO_3 Acid Reacted α-Fe_2O_3 in the Presence of Environmentally Relevant Pressures of Relative Humidity and Molecular Oxygen. The high-resolution spectra of Fe2p, O1s and N1s binding energy regions of unreacted and α-Fe_2O_3 reacted with HNO_3 for 25 min are shown in Figure 2. Assignments of the observed peaks in the different binding energy regions are given in Table 1 with values reported for

Table 1. Assignment of Binding Energies for N1s, O1s, and Fe2p Transitions

		binding energy, eV	
region	assigned species	this work[a]	literature ref
N1s	NO_3^-	407.4	407.4 ($NaNO_3$) Baltrusaitis et al.[28] and 407.3 (NO_3^-) Baltrusaitis et al.[28]
	NO_2^-	not observed	403.6 ($NaNO_2$) Baltrusaitis et al.[28] and 403.1 (NO_2^-) Rosseler et al.[19]
	NO^-	401.7	401.7 (NO^-) Baltrusaitis et al.[28] and 402.6 (NO^-) Overbury et al.[39]
	atomic N^- on defect sites	400.3	400.3 (N^-) Baltrusaitis et al.,[28] 400.5 (anionic N at defects) Overbury et al.;[39] 400.8 (atomic N) Rosseler et al.[19]
	N^{3-}	not observed	397.4 (FeN) Torres et al.[33]
O1s	lattice O in α-Fe_2O_3	530.0	529.8 Baltrusaitis et al.[30]
	chemisorbed NO_3^-	532.5	531.3 Rodriguez et al.[34]
Fe2p	lattice Fe in α-Fe_2O_3	$Fe2_{p3/2}$, 711.2 and Fe $2_{p1/2}$, 724.7	Fe $2_{p3/2}$, 710.8 and Fe $2_{p1/2}$, 724.4 Baltrusaitis et al.[30]

[a]Calibrated to the C1s peak at 285.0 eV.

reference compounds and previous literature assignments. Photoelectrons in the Fe2p region for unreacted α-Fe_2O_3 are at binding energies of 711.2 and 724.7 eV, which correspond to $Fe2_{p3/2}$ and $Fe2_{p1/2}$. In the O1s region, photoelectrons at 530.0 and 531.6 eV were observed for the unreacted surface. These are assigned to Fe−O in α-Fe_2O_3 lattice structure and surface hydroxyl groups, respectively. Upon reaction with HNO_3, formation of adsorbed nitrate is observed as well as seen by a new peak in the N1s region. Additionally, there are observed shifts in the O1s and Fe2p levels by ∼0.5 and ∼0.7 eV, respectively, as a result of strong electrostatic interaction between nitrate and the hematite surface. The peak appearing at 532.5 eV in the O1s region after reacting with HNO_3 can be assigned to the oxygen atoms in adsorbed nitrate. A similar peak has been assigned to chemisorbed nitrate by Rodriguez et al. for NO_2 reacted $TiO_2(110)$ surface.[34] The high-resolution N1s spectrum of HNO_3 reacted α-Fe_2O_3 can be curve fit with one component corresponding to the 407.4 eV peak that is assigned to nitrate ion (NO_3^-), adsorbed on the surface. The binding energy of this peak can be confirmed by the binding energy of $NaNO_3$.[28] The formation of adsorbed NO_3^- species can be written as follows:

$$HNO_3(g) \rightarrow NO_3^-(ads) + H^+(ads) \quad (1)$$

Nitrate formation is governed by dissociative HNO_3 adsorption with NO_3^- occupying Fe sites and dissociated proton on lattice oxygen sites according to reaction 1. Another possible adsorption mechanism is surface hydroxyl groups react with HNO_3 forming adsorbed nitrate and water. Bands for newly formed water or hydroxyl groups were not readily apparent due to overlap with oxygen band of adsorbed nitrate in O1s region of HNO_3 reacted α-Fe_2O_3 as shown in Figure 2. The dissociative adsorption of HNO_3 acid is presumably an exothermic process and thus thermodynamically favorable process on hematite surface. Upon HNO_3 adsorption, no features were observed around 403 or 406 eV region to surface nitrite (NO_2^-) or molecularly adsorbed NO_2 species. Formation of such species has been observed in various oxide surfaces including hematite when reacted with NO_2.[19,28,35,36]

Further experiments were performed by adsorbing HNO_3 on α-Fe_2O_3 particles and then subsequently exposing this reacted surface to various conditions, that is, under dry conditions % RH < 1 and without and with 100 Torr of O_2 as well as 45% RH without and with 100 Torr of O_2. Upon postanalysis with XPS, no new peaks nor change in the binding energy were observed in the N1s upon subjecting HNO_3 reacted α-Fe_2O_3 particles for 30 min under these different environmental conditions.

Nitrate Photochemistry on α-Fe_2O_3 in the Presence of Environmentally Relevant Pressures of Water Vapor and Molecular Oxygen. To understand the photochemistry of adsorbed nitrate on α-Fe_2O_3 particle surfaces following reaction with nitric acid, the surface was irradiated and high-resolution XPS analysis was performed. The high-resolution spectra in the N1s binding energy region of α-Fe_2O_3 reacted with HNO_3 and then irradiated with UV light (λ > 300 nm) for 90 min are shown in Figure 3. These experiments were performed under different levels of molecular oxygen and water vapor. XPS in the N1s showed only the binding energy peak corresponding to surface nitrate at 407.4 eV, but with a decreased intensity following UV exposure time indicating loss of surface bound nitrate. However, when nitrate was irradiated with UV radiation in the presence of water vapor, a broad feature appeared at low

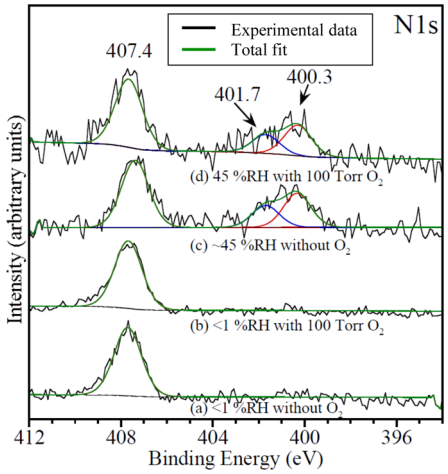

Figure 3. High resolution X-ray photoelectron spectra of α-Fe_2O_3 particles in the N1s binding energy regions following exposure to HNO_3 to saturation coverages and subsequent UV irradiation for 90 minutes in the presence and absence of water vapor and molecular oxygen. (a) %RH < 1 without O_2, (b) %RH < 1 with 100 Torr O_2, (c) %RH = 45 without 100 Torr O_2, (d) %RH = 45 with 100 Torr O_2 at T = 296 K. Black and green lines represent the experimental data acquired and the total fit respectively. Different surface species obtained by peak fitting are shown in red and blue lines. The fitted curve for the nitrate peak overlaps with the total fit.

dx.doi.org/10.1021/jp409017m | J. Phys. Chem. A 2014, 118, 158−166

binding energy region (Figure 3c and d), and there is also a more significant decrease in the intensity of nitrate peak (vide infra). This broad low binding energy feature was fit to two components, a peak centered at 401.7 and another 400.3 eV. The exact binding energy assignment of reduced nitrogen species between 402 and 399 eV has been controversial as the surface binding sites can change the binding energy slightly. Baltrusaitis and co-workers have discussed these differences in detail and used computational analysis to assign these two features at 401.7 and 400.3 eV to NO^- and N^-, respectively.[28]

In previous studies, the formation of NO has been observed using FTIR spectroscopy. This has been proposed to occur via a short-lived NO_2 and/or NO_2^- intermediate according to reactions 2−4.[18]

$$NO_3^-(ads) + H^+ + h\nu \rightarrow NO_2(ads) + OH^\bullet \quad (2)$$

$$NO_3^-(ads) + h\nu \rightarrow NO_2^-(ads) + O(^3P) \quad (3)$$

$$NO_2^-(ads) + H^+ + h\nu \rightarrow NO(ads) + OH^\bullet \quad (4)$$

The newly formed adsorbed NO and NO_2 can subsequently desorb into the gas phase. Photolysis of adsorbed nitrate on alumina reported NO and NO_2 as the major gas-phase species.[18] It has also been shown that NO has a relatively high electron affinity and can easily trap free electron, thus forming a negatively charged NO^- anion adsorbed on metal cationic sites on the surface according to reaction 5, resulting in a band at 401.7 eV.[28]

$$NO(ads) + e^- \rightarrow NO^-(ads) \quad (5)$$

$$O(vacancy)^- + NO(ads) \rightarrow N^-(ads) + O(ads) \quad (6)$$

In addition, adsorbed NO can decompose to produce atomic N and O on the surface as reported by NO_2 adsorption studies on Mo(110) by Jirsak et al.[37] In another study, adsorbed NO conversion to N_2O through an atomic N intermediate has been reported on TiO_2 surfaces.[38] Rosseler et al. have observed a band at 400.8 eV for NO_2 adsorption on TiO_2 studies and have assigned it to reduced N. Overbury et al. have observed a band at 400.5 eV that they have claimed to anionic N species that have resulted from NO decomposition, which then had charge transferred to nitrogen atom leading to N^-.[39] Iron oxide surfaces have been reported as being rich with oxygen vacancies. Higher population of point defects has been reported for hematite surface as compared to the bulk.[40] Furthermore, oxygen vacancies on other semiconductor surfaces like TiO_2 have shown negative charge associated with trapped electrons, and similar sites have been proposed on iron oxide surfaces in previous studies.[30,41] The electrons generated from band gap excitations of hematite can be trapped in oxygen vacancy sites and increase the availability of negatively charged oxygen vacancy sites. Therefore, in the current study, newly formed NO decomposition on negatively charged O vacancy can be expected, resulting in N^- according to reaction 6.

More reaction pathways (reactions 7−9) are available for nitrate photolysis on a semiconductor surface as evident by the nitrate photochemistry studies on TiO_2.[20] Nitrate photolysis via a nitrate radical intermediate forming reduced NO and NO_2 was reported for TiO_2 surfaces.[42] These reactions, initiated by electron−hole (e^-/h^+) pairs, can also play a significant role on the hematite surface.

$$NO_3^-(ads) + h^+ \rightarrow NO_3^\bullet \quad (7)$$

$$NO_3^\bullet + h\nu \rightarrow NO(ads) + O_2 \quad (8)$$

$$NO_3^\bullet + h\nu \rightarrow NO_2(ads) + O^\bullet \quad (9)$$

$$NO_2(ads) + e^- \rightarrow NO_2^- \quad (10)$$

Newly formed NO_2(ads) from reaction 9 can either react with photogenerated electrons forming adsorbed NO_2^-, which undergoes continued photoreactions to yield adsorbed NO according to reaction 4, or desorb to the gas phase. However, from these studies, we have no evidence for NO_2(ads) or NO_2^-(ads). Therefore, NO_2(ads) conversion to NO(ads) via NO_2^- may be a very fast reaction. Additionally, the electron attachment, reaction 10, is more feasible on the hematite surface due to the availability of photogenerated electrons.

Figure 4 shows the high-resolution spectra in the N1s region for α-Fe_2O_3 surface exposed to gas-phase HNO_3 and then

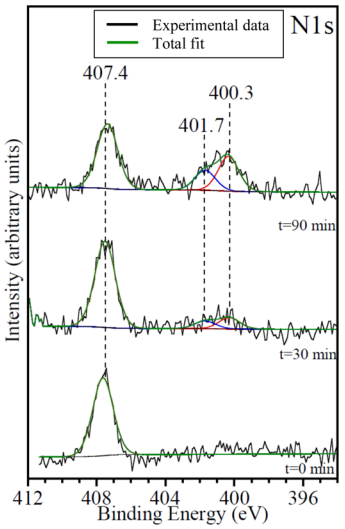

Figure 4. High-resolution X-ray photoelectron spectra of α-Fe_2O_3 particles in the N1s binding energy regions following exposure to HNO_3 to saturation coverages and subsequent UV irradiation for 0, 30, and 90 min in the presence of %RH = 45 without O_2. All spectra were acquired at 296 K. Black and green lines represent the experimental data acquired and the total fit, respectively. Surface species obtained by peak fitting are shown in red and blue lines. The fitted curve for nitrate peak overlaps with the total fit.

irradiated with UV light for 0, 30, and 90 min time periods in the presence of 45% RH. Spectra clearly show the loss of surface-bound nitrate and the appearance of low binding energy features corresponding to reduced nitrogen species with increasing irradiation time. Reduced-nitrogen, surface-species formation did not show any difference in the presence of molecular oxygen (spectra not shown). In the presence of water vapor, hydroxyl radicals formed on hematite surface upon UV irradiation (reaction 11) can initiate the following reactions in competition with the nitrate photolysis reactions leading to secondary pathways:

$$H_2O + h^+ \rightarrow H^+ + OH^\bullet \quad (11)$$

$$NO_2^- + H^+ \rightarrow HONO \quad (12)$$

$$NO_2^- + OH^\bullet \rightarrow NO_2 + OH^- \quad (13)$$

$$NO_3^-(ads) + OH^\bullet \rightarrow NO_3^\bullet + OH^- \quad (14)$$

dx.doi.org/10.1021/jp409017m | J. Phys. Chem. A 2014, 118, 158−166

These alternative pathways can dominate in the presence of relative humidity according to reactions 12 and 13 converting NO_2^- intermediate to the gas-phase HONO and NO_2 and converting NO_3^- (ads) to nitrate radical (reaction 14).[20,42] In HONO uptake studies on Fe_2O_3, Bedjanian and co-workers have reported the HONO decomposition to gas-phase NO and NO_2.[43] This decomposition is also possible under the experimental conditions used in the current study.

Surface product formation under irradiation was investigated as a function of water vapor pressure. It can be seen that the formation of surface-bound reduced nitrogen species changes significantly with water vapor pressure. The left panel of Figure 5 shows the N1s region of HNO_3 reacted α-Fe_2O_3 after 90 min

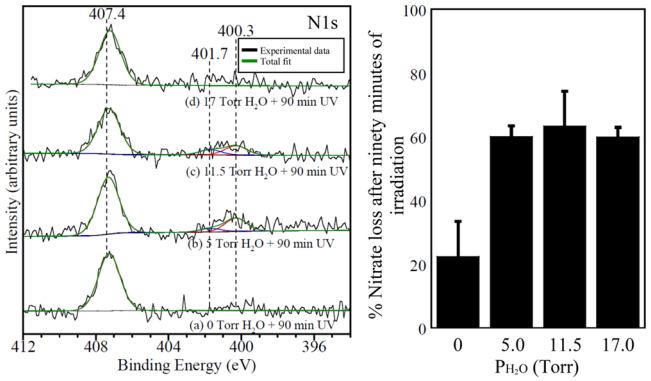

Figure 5. High-resolution X-ray photoelectron spectra of α-Fe_2O_3 particles in the N1s binding energy regions following exposure to HNO_3 to saturation coverages and subsequent UV irradiation for 90 min in the presence of (a) 0 Torr H_2O, (b) 5 Torr H_2O, (c) 11.5 Torr H_2O, and (d) 17 Torr H_2O at T = 296 K (left panel) and the percentage loss of nitrate after 90 min of UV irradiation in the presence of different water vapor pressures (right panel). In the left panel, black and green lines represent the experimental data acquired and the total fit, respectively. Surface species obtained by peak fitting are shown as red and blue lines. The fitted curve for nitrate peak overlaps with the total fit.

UV irradiation at different water vapor pressures. UV irradiation in the presence of different water vapor pressures showed changes in the presence of reduced nitrogen surface species. The right panel of Figure 5 shows the total nitrate loss after 90 min UV irradiation calculated from initial and final N1s:Fe2p speciation ratio using the adsorbed nitrate N1s peak at 407.4 eV. In the absence of water vapor, reduced nitrogen species were not observed. This can be due to the low nitrate loss under irradiation in the absence of water vapor and low availability of electrons due to higher electron hole recombination. As shown in the right panel, the total nitrate loss is ~3 times higher in the presence of water vapor. This confirms the important role of water in nitrate photolysis on hematite and the increase in nitrate loss due to increase ability to react and new mechanisms available for reactions, giving rise to a significantly greater loss of nitrate and the observed increase in surface-bound products at 5 and 11.5 Torr water exposures. Additionally, in the presence of water vapor, photogenerated holes react with water molecules, and that decreases the e^-/h^+ recombination leaving more electrons to form reduced nitrogen surface species. In the presence of water vapor, around 60% nitrate loss was observed for all three %RH experiments. However, reduced-nitrogen, surface-species were not observed at the highest water vapor exposure. This may suggest that surface sites for NO^- and N^- adsorption are available only at 5 and 11.5 Torr water exposures (24% and 55% RH) and potentially covered at the highest water vapor pressure of 17 Torr (81% RH). Mogili and co-workers have previously reported that the water adsorption is not uniform on hematite surfaces, and water adsorption results in water patches leaving some of the surface sites available up to 60% RH water vapor exposure.[44] This uneven water adsorption has been discussed in several previous studies.[44−46] Because the percentage nitrate loss did not show much difference for three water vapor pressures, the disappearance of NO^- and atomic N^- species at the highest water vapor exposure can be possibly due to the occupation of water molecules on adsorption sites at the highest relative humidity that are then blocked for further reaction.

Figure 6 shows a schematic of the reactions occurring for nitrate photochemistry on hematite surfaces. In particular, the schematic shows the formation of reduced nitrogen surface species and gas-phase NO, NO_2 formation under different water vapor exposures. Additionally, Table 2 contains the average number of water layers on the hematite surface as a function of relative humidity as reported by Mogili et al. for α-Fe_2O_3.[44] These estimates do not represent the dynamic nature or in some cases "islanding and clustering" of water or regions that contain no adsorbed water.

In the absence of water vapor, low nitrate loss and higher e^-/h^+ recombination are seen to not facilitate reduced nitrogen surface species formation. At intermediate and higher water vapor pressures, higher nitrate loss results due to the available new mechanisms in the presence of water molecules. In the presence of water vapor, oxide coordinated nitrate converts to water solvated nitrate, and the degree of solvation depends on the amount of water vapor equilibrium with the surface. At the intermediate water vapor exposures of 5 and 11.5 Torr (24% and 55% RH), ~2 and ~3 water layers are formed. In these intermediate water vapor exposures, less electron hole recombination due to water molecules reaction with photogenerated holes and availability of adsorption sites results in reduced nitrogen surface species. At the highest water vapor pressure, the surface is covered with ~4 layers of water, and adsorption sites are not readily available for the formation of reduced nitrogen surface species to any great extent.

The gas-phase products formed during photolysis of nitrate adsorbed on α-Fe_2O_3 particles were also monitored using the FTIR system described in the Experimental Methods. Adsorption of HNO_3 on α-Fe_2O_3 particles produced absorption bands for monodentate, bidentate and bridged nitrate in the FTIR spectrum under dry conditions. Adsorbed nitrate exposed to water vapor showed the formation of solvated nitrate. Surface FTIR spectra were consistent with data reported for HNO_3 adsorption on α-Fe_2O_3 under dry and wet conditions. Adsorbed nitrates on nanoparticle surfaces such as γ-Fe_2O_3, γ-Al_2O_3, α-Al_2O_3 have been reported in previous publications.[32,47,48] Figure 7 show the gas-phase product formation recorded as a function of UV exposure time in the presence of 45% RH of water vapor. Three peaks appeared at 1616, 1874, and 2223 cm^{-1}. These vibrational modes can be attributed to the gas-phase NO_2, NO and N_2O species, respectively. Mechanisms for N_2O formation are discussed below. The bands for gas-phase NO and N_2O appeared after 30 min UV irradiation and grow continuously for 420 min. Gas-phase NO_2 was not observed after 30 min irradiation and can be due to the NO_2 reaction with H_2O according to reaction 15

dx.doi.org/10.1021/jp409017m | J. Phys. Chem. A 2014, 118, 158−166

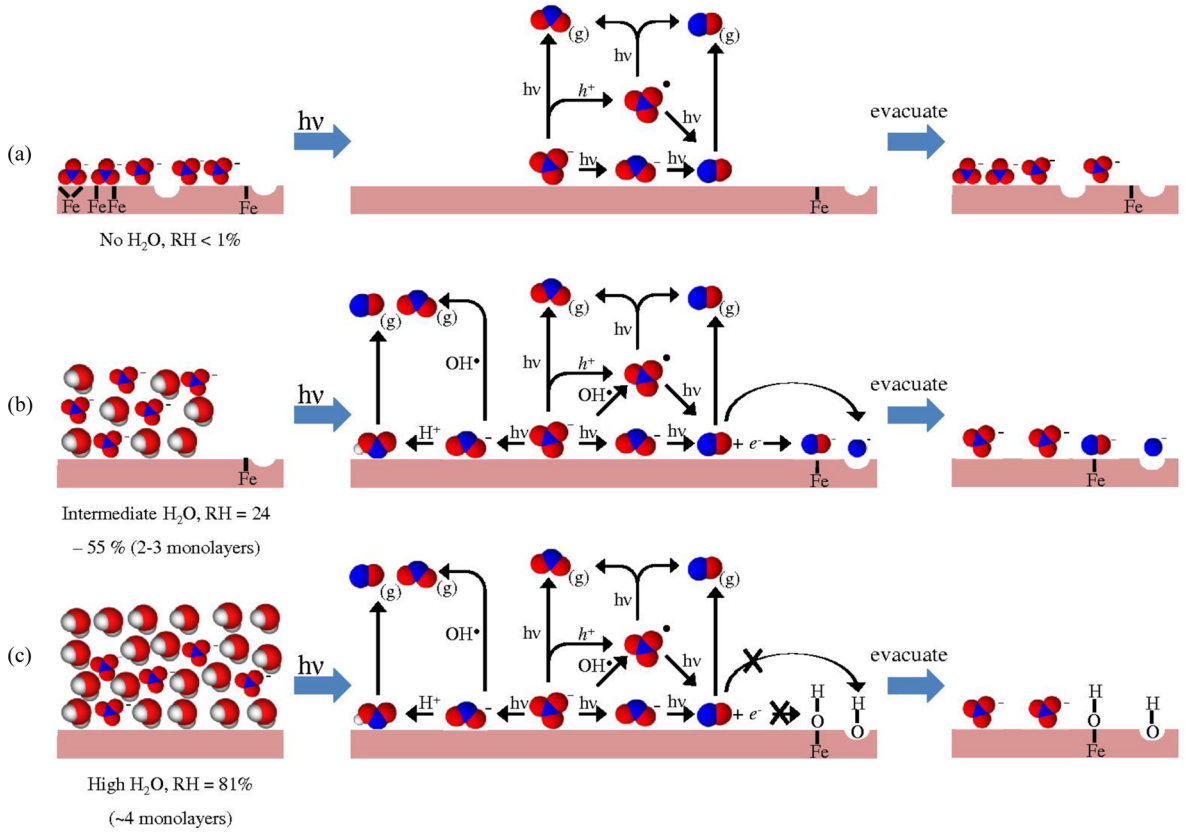

Figure 6. Schematic of adsorbed nitrate photochemistry on α-Fe_2O_3; (a) in the absence of water vapor, adsorbed nitrates present on the hematite surface in different coordination modes undergo limited nitrate photochemistry due to electron and hole pair recombination, (b) in the presence of 5 and 11.5 Torr water vapor pressure (24 and 55 %RH), there is higher nitrate conversion due to lower electron/hole recombination rates, thus NO^- and N^- form on cationic sites and O vacancy sites, (c) in the presence of 17 Torr (81 %RH) of water vapor pressure, there is high nitrate conversion, similar as in (b), however cationic sites and O vacancy sites are not available to form NO^- and N^-. See text for further details.

Table 2. Estimated Adsorbed Water Layers on α-Fe_2O_3 as a Function of Water Relative Humidity from Water Adsorption Isotherm Curves[a]

%RH	estimate of number of water layers
10	1
30	2
60	3
75	4

[a]See ref 44.

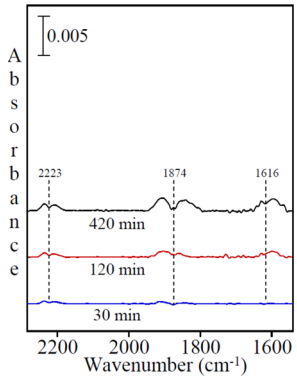

Figure 7. Transmission FTIR spectra of gas-phase product formation from UV illumination of adsorbed nitrate under 45% RH in the absence of O_2 at T = 296 K.

under acidic conditions. Another possible reaction is NO_2 reacts with H_2O forming HONO and HNO_3 according to reaction 16.[49]

$$8NO_2 + 3H_2O \rightarrow N_2O + 6HNO_3 \quad (15)$$

Gas-phase HONO was not observed possibly due to its decomposition on Fe_2O_3 particle surfaces. Gas-phase NO_2 appeared at longer irradiation times of 120 and 420 min. The dominant gas-phase species in the presence of water vapor was NO at all of the irradiation times agreeing with the presence of adsorbed NO^- on the surface. Identical experiments performed to monitor the gas-phase products under wet condition, in the presence of molecular oxygen, showed higher gas-phase NO_2 amounts (data not shown). The presence of molecular oxygen has shown NO_2 dominance in the gas phase on UV irradiation of nitrated Al_2O_3 and TiO_2 surfaces.[47,50] This has been explained by two NO molecules that react with molecular oxygen to form two NO_2 molecules.

These infrared spectra clearly indicate that only NO and NO_2 as the major gas-phase products and small amount of N_2O are present in the system even after irradiating HNO_3 reacted surface for 420 min. The N_2O formation in the presence of 45% RH can be due to the secondary pathway according to reaction 15 under acidic conditions in the presence of water vapor.[51] Furthermore, reactions 17 and 18 can be sources for N_2O as well.[52]

$$2NO_2 + H_2O \rightarrow HONO + HNO_3 \quad (16)$$

dx.doi.org/10.1021/jp409017m | J. Phys. Chem. A 2014, 118, 158–166

$$NO + NO_3^- \rightarrow N_2O + 5/4O_2 + 1/2O^{2-} \quad (17)$$

$$NO_2 + NO_3^- \rightarrow N_2O + 7/4O_2 + 1/2O^{2-} \quad (18)$$

Aqueous Phase Behavior of HNO_3 Reacted Hematite Particles. HNO_3 reacted α-Fe_2O_3 particles were introduced to aqueous solutions to investigate possible enhancements in Fe dissolution due to HNO_3 uptake. Studies have shown HNO_3 reacted α-FeOOH formed stable suspension as compared to α-FeOOH that was not reacted.[53] Sedimentation plots of HNO_3 reacted and unreacted α-Fe_2O_3 showed fast settling with no difference between the two. Dissolved Fe concentration was below the limit of detection of ICP(OES). The data explain the HNO_3 reaction does not change particle aggregation or enhance Fe dissolution from α-Fe_2O_3 particles.

Conclusions and Atmospheric Implications. HNO_3 adsorption on hematite surface under different environmental conditions of relative humidity and molecular oxygen was explored in the presence and absence of UV irradiation. Ex and in situ analyses were used to follow the surface and gas-phase species that form in these reactions. Surface nitrate was found to be the predominant species in the absence of UV irradiation. Irradiation with UV light resulted in the formation of surface-bound, reduced-nitrogen species. Furthermore, XPS analysis indicates that reduced species are observed only with the presence of coadsorbed water except at the highest pressures of water vapor, and thus highest coverage, during the UV irradiation. Thus, these data show a relative humidity dependent extent of reaction and the stability of reduced surface species that form. Transmission FTIR studies confirm that irradiation with the UV light resulted in the reduction of the adsorbed nitrate to form gas-phase N_2O, NO, and NO_2 species. The distribution of surface-bound and gas-phase products depends on the presence of water vapor. Additionally, HNO_3 acid adsorption does not change the dissolution and solution phase behavior of these α-Fe_2O_3 particles.

The data presented here support the role that iron-containing aerosol surfaces in the atmosphere can facilitate the conversion of adsorbed nitrate to gas-phase NO_2, NO, and N_2O as well as adsorbed NO^- and N^- during heterogeneous photochemistry. The effect of relative humidity in the formation of highly reduced nitrogen species on iron oxides has not been shown previously and represents another role of adsorbed water in the reaction chemistry of environmental interfaces.

■ ASSOCIATED CONTENT

Supporting Information

Figure S1: (a) X-ray diffraction pattern and (b) scanning electron microscope image of α-Fe_2O_3. Complete author list of ref 2. This material is available free of charge via the Internet at http://pubs.acs.org.

■ AUTHOR INFORMATION

Corresponding Author

*Phone: 319-335-1392. E-mail: vicki-grassian@uiowa.edu.

Author Contributions

‖These authors contributed equally.

Notes

The authors declare no competing financial interest.

■ ACKNOWLEDGMENTS

This material is based on the work supported by the National Science Foundation under grant CHE-0952605. Any opinions, findings, and conclusions or recommendations expressed in this material are those of the authors and do not necessarily reflect the views of the National Science Foundation.

■ REFERENCES

(1) Cwiertny, D. M.; Young, M. A.; Grassian, V. H. Chemistry and Photochemistry of Mineral Dust Aerosol. *Annu. Rev. Anal. Chem.* **2008**, *59*, 27−51.

(2) Yu, Y.; Ezell, M. J.; Zelenyuk, A.; Imre, D.; Alexander, L.; Ortega, J.; Thomas, J. L.; Gogna, K.; Tobias, D. J.; D'Anna, B.; et al. Nitrate Ion Photochemistry at Interfaces: A New Mechanism for Oxidation of α-pinene. *Phys. Chem. Chem. Phys.* **2008**, *10*, 3063−3071.

(3) Jacobi, H. W.; Annor, T.; Quansah, E. Investigation of The Photochemical Decomposition of Nitrate, Hydrogen Peroxide, and Formaldehyde in Artificial Snow. *J. Photochem. Photobiol., A* **2006**, *179*, 330−338.

(4) Honrath, R. E.; Peterson, M. C.; Guo, S.; Dibb, J. E.; Shepson, P. B.; Campbell, B. Evidence of NO_x Production Within or Upon Ice Particles in the Greenland Snowpack. *Geophys. Res. Lett.* **1999**, *26*, 695−698.

(5) Jones, A. E.; Weller, R.; Wolff, E. W.; Jacobi, H. W. Speciation and Rate of Photochemical NO and NO_2 Production in Antarctic Snow. *Geophys. Res. Lett.* **2000**, *27*, 345−348.

(6) Honrath, R. E.; Peterson, M. C.; Dziobak, M. P.; Dibb, J. E.; Arsenault, M. A.; Green, S. A. Release of NO_x from Sunlight-irradiated Midlatitude Snow. *Geophys. Res. Lett.* **2000**, *27*, 2237−2240.

(7) Mack, J.; Bolton, J. R. Photochemistry of Nitrite and Nitrate in Aqueous Solution: A Review. *J. Photochem. Photobiol., A* **1999**, *128*, 1−13.

(8) Hudson, P. K.; Schwarz, J.; Baltrusaitis, J.; Gibson, E. R.; Grassian, V. H. A Spectroscopic Study of Atmospherically Relevant Concentrated Aqueous Nitrate Solutions. *J. Phys. Chem. A* **2007**, *111*, 544−548.

(9) Minero, C.; Chiron, S.; Falletti, G.; Maurino, V.; Pelizzetti, E.; Ajassa, R.; Carlotti, M.; Vione, D. Photochemincal Processes Involving Nitrite in Surface Water Samples. *Aquat. Sci.* **2007**, *69*, 71−85.

(10) Goldstein, S.; Rabani, J. Mechanism of Nitrite Formation by Nitrate Photolysis in Aqueous Solutions: The Role of Peroxynitrite, Nitrogen Dioxide and Hydroxyl Radical. *J. Am. Chem. Soc.* **2007**, *129*, 10597−10601.

(11) Dubowski, Y.; Sumner, A. L.; Menke, E. J.; Gaspar, D. J.; Newberg, J. T.; Hoffman, R. C.; Penner, R. M.; Hemminger, J. C.; Finlayson-Pitts, B. J. Interactions of Gaseous Nitric Acid with Surfaces of Environmental Interest. *Phys. Chem. Chem. Phys.* **2004**, *6*, 3879−3888.

(12) Rivera-Figueroa, A. M.; Sumner, A. L.; Finlayson-Pitts, B. J. Laboratory Studies of Potential Mechanisms of Renoxification of Tropospheric Nitric Acid. *Environ. Sci. Technol.* **2003**, *37*, 548−554.

(13) Baergen, A. M.; Donaldson, D. J. Photochemical Renoxification of Nitric Acid on Real Urban Grime. *Environ. Sci. Technol.* **2013**, *47*, 815−820.

(14) Moussa, S. G.; Stern, A. C.; Raff, J. D.; Dilbeck, C. W.; Tobias, D. J.; Finlayson-Pitts, B. J. Experimental and Theoretical Studies of the Interaction of Gas Phase Nitric Acid and Water with a Self-assembled Monolayer. *Phys. Chem. Chem. Phys.* **2013**, *15*, 448−458.

(15) Frinak, E. K.; Wermeille, S. J.; Mashburn, C. D.; Tolbert, M. A.; Pursell, C. J. Heterogeneous Reaction of Gaseous Nitric Acid on γ-Phase Iron(III) Oxide. *J. Phys. Chem. A* **2004**, *108*, 1560−1566.

(16) Mashburn, C. D.; Frinak, E. K.; Tolbert, M. A. Heterogeneous Uptake of Nitric Acid on Na-Montmorillonite Clay as a Function of Relative Humidity. *J. Geophys. Res.: Atmos.* **2006**, *111*, D15213.

(17) Gankanda, A.; Grassian, V. H. Nitrate Photochemistry in NaY Zeolite: Product Formation and Product Stability under Different Environmental Conditions. *J. Phys. Chem. A* **2013**, *117*, 2205−2212.

(18) Rubasinghege, G.; Grassian, V. H. Photochemistry of Adsorbed Nitrate on Aluminum Oxide Particle Surfaces. *J. Phys. Chem. A* **2009**, *113*, 7818−7825.
(19) Rosseler, O.; Sleiman, M.; Montesinos, V. N.; Shavorskiy, A.; Keller, V.; Keller, N.; Litter, M. I.; Bluhm, H.; Salmeron, M.; Destaillats, H. Chemistry of NO_x on TiO_2 Surfaces Studied by Ambient Pressure XPS: Products, Effect of UV Irradiation, Water, and Coadsorbed K^+. *J. Phys. Chem. Lett.* **2013**, *4*, 536−541.
(20) Bedjanian, Y.; El Zein, A. Interaction of NO_2 with TiO_2 Surface Under UV Irradiation: Products Study. *J. Phys. Chem. A* **2012**, *116*, 1758−1764.
(21) Kleffmann, J. Daytime Sources of Nitrous Acid (HONO) in the Atmospheric Boundary Layer. *ChemPhysChem* **2007**, *8*, 1137−1144.
(22) Nishino, N.; Finlayson-Pitts, B. J. Thermal and Photochemical Reactions of NO_2 on Chromium(III) Oxide Surfaces at Atmospheric Pressure. *Phys. Chem. Chem. Phys.* **2012**, *14*, 15840−15848.
(23) Hadjiivanov, K.; Bushev, V.; Kantcheva, M.; Klissurski, D. Infrared Spectroscopy Study of the Species Arising During Nitrogen Dioxide Adsorption on Titania (anatase). *Langmuir* **1994**, *10*, 464−471.
(24) Hadjiivanov, K.; Knozinger, H. Species Formed After NO Adsorption and NO+O_2 Co-adsorption on TiO_2: An FTIR Spectroscopic Study. *Phys. Chem. Chem. Phys.* **2000**, *2*, 2803−2806.
(25) Usher, C. R.; Michel, A. E.; Grassian, V. H. Reactions on Mineral Dust. *Chem. Rev.* **2003**, *103*, 4883−4940.
(26) Schwertmann, U.; Cornell, R. M. *Iron Oxides: Structure, Properties, Reactions, Occurences and Uses*, 2nd ed.; Wiley-VCH: Hoboken, NJ, 2007.
(27) Shi, Z.; Krom, M. D.; Jickells, T. D.; Bonneville, S.; Carslaw, K. S.; Mihalopoulos, N.; Baker, A. R.; Benning, L. G. Impacts on Iron Solubility in the Mineral Dust by Processes in the Source Region and the Atmosphere: A Review. *Aeo. Res.* **2012**, *5*, 21−42.
(28) Baltrusaitis, J.; Jayaweera, P. M.; Grassian, V. H. XPS Study of Nitrogen Dioxide Adsorption on Metal Oxide Particle Surfaces Under Different Environmental Conditions. *Phys. Chem. Chem. Phys.* **2009**, *11*, 8295−8305.
(29) Baltrusaitis, J.; Usher, C. R.; Grassian, V. H. Reactions of Sulfur Dioxide on Calcium Carbonate Single Crystal and Particle Surfaces at the Adsorbed Water Carbonate Interface. *Phys. Chem. Chem. Phys.* **2007**, *9*, 3011−3024.
(30) Baltrusaitis, J.; Cwiertny, D. M.; Grassian, V. H. Adsorption of Sulfur Dioxide on Hematite and Goethite Particle Surfaces. *Phys. Chem. Chem. Phys.* **2007**, *9*, 5542−5554.
(31) Fairley, N. CasaXPS 2.3.14, 1999−2008.
(32) Goodman, A. L.; Bernard, E. T.; Grassian, V. H. Spectroscopic Study of Nitric Acid and Water Adsorption on Oxide Particles: Enhanced Nitric Acid Uptake Kinetics in the Presence of Adsorbed Water. *J. Phys. Chem. A* **2001**, *105*, 6443−6457.
(33) Torres, J.; Perry, C. C.; Bransfield, S. J.; Fairbrother, D. H. Low-Temperature Oxidation of Nitrided Iron Surfaces. *J. Phys. Chem. B* **2003**, *107*, 5558−5567.
(34) Rodriguez, J. A.; Jirsak, T.; Liu, G.; Hrbek, J.; Dvorak, J.; Maiti, A. Chemistry of NO_2 on Oxide Surfaces: Formation of NO_3 on TiO_2(110) and NO_2↔O Vacancy Interactions. *J. Am. Chem. Soc.* **2001**, *123*, 9597−9605.
(35) Schmitz, P. J.; Baird, R. J. NO and NO_2 Adsorption on Barium Oxide: Model Study of the Trapping Stage of NO_x Conversion via Lean NO_x Traps. *J. Phys. Chem. B* **2002**, *106*, 4172−4180.
(36) Haubrich, J.; Quiller, R. G.; Benz, L.; Liu, Z.; Friend, C. M. In Situ Ambient Pressure Studies of the Chemistry of NO_2 and Water on Rutile TiO_2(110). *Langmuir* **2010**, *26*, 2445−2451.
(37) Jirsak, T.; Kuhn, M.; Rodriguez, J. A. Chemistry of NO_2 on Mo(110): Decomposition Reactions and Formation of MoO_2. *Surf. Sci.* **2000**, *457*, 254−266.
(38) Rusu, C. N.; Yates, J. T. Photochemistry of NO Chemisorbed on TiO_2(110) and TiO_2 Powders. *J. Phys. Chem. B* **2000**, *104*, 1729−1737.
(39) Overbury, S. H.; Mullins, D. R.; Huntley, D. R.; Kundakovic, L. Chemisorption and Reaction of NO and N_2O on Oxidized and Reduced Ceria Surfaces Studied by Soft X-Ray Photoemission Spectroscopy and Desorption Spectroscopy. *J. Catal.* **1999**, *186*, 296−309.
(40) Warschkow, O.; Ellis, D. E.; Hwang, J.; Mansourian-Hadavi, N.; Mason, T. O. Defects and Charge Transport near the Hematite (0001) Surface: An Atomistic Study of Oxygen Vacancies. *J. Am. Ceram. Soc.* **2002**, *85*, 213−220.
(41) Henderson, M. A. Evidence for Bicarbonate Formation on Vacuum Annealed TiO_2(110) Resulting from a Precursor-mediated Interaction Between CO_2 and H_2O. *Surf. Sci.* **1998**, *400*, 203−219.
(42) Ndour, M.; Conchon, P.; D'Anna, B.; Ka, O.; George, C. Photochemistry of Mineral Dust Surface as a Potential Atmospheric Renoxification Process. *Geophys. Res. Lett.* **2009**, *36*, L05816.
(43) El Zein, A.; Romanias, M. N.; Bedjanian, Y. Kinetics and Products of Heterogeneous Reaction of HONO with Fe_2O_3 and Arizona Test Dust. *Environ. Sci. Technol.* **2013**, *47*, 6325−6331.
(44) Mogili, P. K.; Kleiber, P. D.; Young, M. A.; Grassian, V. H. Heterogeneous Uptake of Ozone on Reactive Components of Mineral Dust Aerosol: An Environmental Aerosol Reaction Chamber Study. *J. Phys. Chem. A* **2006**, *110*, 13799−13807.
(45) Chen, H.; Stanier, C. O.; Young, M. A.; Grassian, V. H. A Kinetic Study of Ozone Decomposition on Illuminated Oxide Surfaces. *J. Phys. Chem. A* **2011**, *115*, 11979−11987.
(46) Rubasinghege, G.; Grassian, V. H. Role(s) of Adsorbed Water in the Surface Chemistry of Environmental Interfaces. *Chem. Commun.* **2013**, *49*, 3071−3094.
(47) Schuttlefield, J.; Rubasinghege, G.; El-Maazawi, M.; Bone, J.; Grassian, V. H. Photochemistry of Adsorbed Nitrate. *J. Am. Chem. Soc.* **2008**, *130*, 12210−12211.
(48) Baltrusaitis, J.; Schuttlefield, J.; Jensen, J. H.; Grassian, V. H. FTIR Spectroscopy Combined with Quantum Chemical Calculations to Investigate Adsorbed Nitrate on Aluminium Oxide Surfaces in the Presence and Absence of Co-adsorbed Water. *Phys. Chem. Chem. Phys.* **2007**, *9*, 4970−4980.
(49) Finlayson-Pitts, B. J.; Wingen, L. M.; Sumner, A. L.; Syomin, D.; Ramazan, K. A. The Heterogeneous Hydrolysis of NO_2 in Laboratory Systems and in Outdoor and Indoor Atmospheres: An Integrated Mechanism. *Phys. Chem. Chem. Phys.* **2003**, *5*, 223−242.
(50) Monge, M. E.; D'Anna, B.; George, C. Nitrogen Dioxide Removal and Nitrous Acid Formation on Titanium Oxide Surfaces-An Air Quality Remediation Process? *Phys. Chem. Chem. Phys.* **2010**, *12*, 8991−8998.
(51) Wiesen, P.; Kleffmann, J.; Kurtenbach, R.; Becker, K. H. Mechanistic Study of the Heterogeneous Conversion of NO_2 into HONO and N_2O on Acid Surfaces. *Faraday Discuss.* **1995**, *100*, 121−127.
(52) Malecki, A.; Maleka, B. Formation of N_2O During Thermal Decomposition of d-metal Hydrates Nitrates. *Thermochim. Acta* **2006**, *446*, 113−116.
(53) Wijenayaka, L. A.; Rubasinghege, G.; Baltrusaitis, J.; Grassian, V. H. Surface Chemistry of α-FeOOH Nanorods and Microrods with Gas-Phase Nitric Acid and Water Vapor: Insights into the Role of Particle Size, Surface Structure, and Surface Hydroxyl Groups in the Adsorption and Reactivity of α-FeOOH with Atmospheric Gases. *J. Phys. Chem. C* **2012**, *116*, 12566−12577.